TECHNICAL REPORT • OPEN ACCESS

X-ray spectroscopy with a photon-counting SiPM-based scintillation detector

Jinst

PUBLISHED BY IOP PUBLISHING FOR SISSA MEDIALAB

RECEIVED: *March 30, 2023*
REVISED: *June 13, 2023*
ACCEPTED: *September 4, 2023*
PUBLISHED: *September 29, 2023*

TECHNICAL REPORT

2023 JINST 18 T09007

X-ray spectroscopy with a photon-counting SiPM-based scintillation detector

S. Ceravolo,[c] **R. Gargiulo,**[a,c,*] **D. Paesani,**[b] **A. Russo**[c] **and I. Sarra**[c]

[a] *Università degli studi di Roma — La Sapienza, Piazzale Aldo Moro 5, Rome, Italy*
[b] *Università degli studi di Roma — Tor Vergata, Via Cracovia, Rome, Italy*
[c] *Laboratori Nazionali di Frascati, Via Enrico Fermi 54, Frascati, Italy*

E-mail: ruben.gargiulo@uniroma1.it

ABSTRACT: A new low-energy X-ray detector was built and operated, using a plastic scintillator coupled to a large area SiPM. The signal is amplified with a low-noise, high gain, custom circuit providing excellent photon-counting capabilities and allowing a quasi-digital measurement. The detector was tested using X-rays coming from molybdenum K lines (17.4 and 19.6 keV), and an energy resolution of 28% is obtained with 20 photoelectrons per X-ray photon on average.

KEYWORDS: X-ray detectors; Photon detectors for UV, visible and IR photons (solid-state)

*Corresponding author.

https://doi.org/10.1088/1748-0221/18/09/T09007

Contents

2023 JINST 18 T09007

1 Introduction

Plastic scintillators were invented in the 1950s and they are now employed in a wide range of particle detectors. Nowadays many plastic scintillators, for example EJ-200 [1], can provide a high light yield (about 10^4 photons/MeV) with fast emission times (less than 1 ns) and a few ns decay times, combined with relatively low prices and availability in a huge variety of shapes and sizes. They are mainly employed for detection of charged particles and have a very large interaction length of $\lambda = 14$ cm for 1 MeV gamma rays. The photon interaction length begins to decrease to $\lambda = 5$ cm for energies below 50 keV and is dominated by photoelectric effect below 10 keV, reaching $\lambda = 1$ mm at 6 keV [2]. Efficient detection of X-rays in the 5-50 keV range is then feasible using plastic scintillators with thicknesses ranging from a few mm to tens of cm. In the high end of this energy range (near 50 keV) recent studies showed that an energy resolution of the order of 20% (with a $1/\sqrt{E}$ scaling) is achievable [3]. In order to test the performances of plastic scintillators at lower energies (near 20 keV), we built and operated an X-ray detector based on a EJ-200 plastic scintillator provided by Eljen Technology, coupled to a SiPM providing single-photon counting capabilities [4].

2 Detector

The detector is composed of a 6.5×6.5×5 mm^3 EJ-200 polyvinyl-toluene-based plastic scintillator provided by Eljen Technology, coupled with optical grease to a 6×6 mm^2 Hamamatsu S13360-6050CS SiPM. The SiPM signal is amplified with a low-noise custom circuit providing a ×600 gain. Thanks to the amplifier performances, the system has optical photon-counting capabilities, reaching pulse amplitudes (charges) of 80 mV (200 pC) for a single photoelectron. Then, the different peaks corresponding to the photo-electron countings can be easily distinguished in the charge spectrum up to 30 photoelectrons, allowing a quasi-digital measurement.

A polyvinyl-toluene-based plastic scintillator material (EJ-200) has been chosen for its high light yield and fast emission.

EJ-200 has a high scintillation efficiency (10000 photons per deposited MeV) and an emission spectrum peaking at 425 nm (in the blue region), as shown in figure 1.

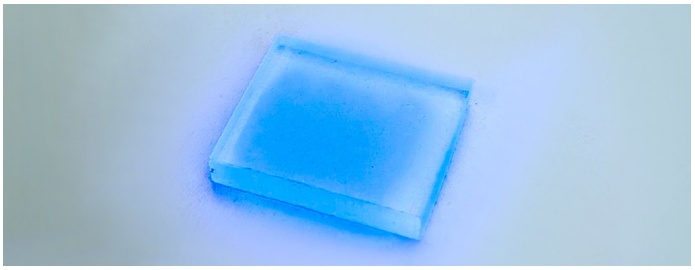

Figure 1. Picture of an EJ-200 scintillator showing blue emission under UV light.

Furthermore, the selection of EJ-200 grants a very fast (0.9 ns) optical rise time and 2.1 ns decay time. The scintillator size is large enough to completely absorb the electrons ejected by photoelectric effect, which have a range less than 50 µm [5]. The X-ray interaction probability with the detector P is limited by the scintillator thickness t, as follows:

$$P = 1 - e^{-t/L} \tag{2.1}$$

where L is the X-ray absorption length in polyvinyl-toluene (see figure 2).

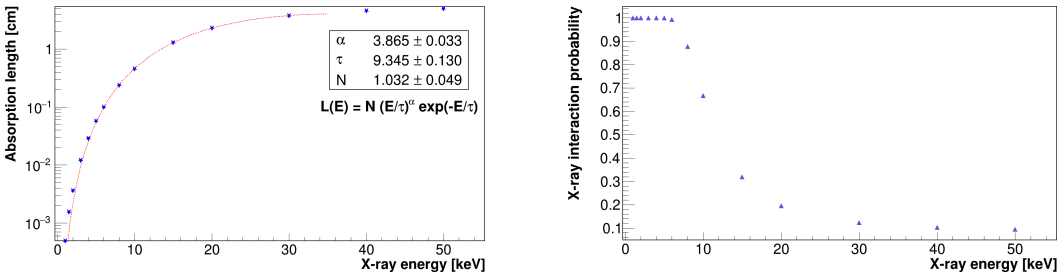

Figure 2. X-ray absorption length for EJ-200 vs. energy, fitted with an empirical formula in order to interpolate the data (left) and interaction probability for a 0.5 cm thick EJ-200 scintillator vs. energy (right) [6].

As shown in figure 2, at energies greater than 10 keV the efficiency of our system drops significantly, so a scintillator with higher Z or larger thickness should be employed. The scintillator is wrapped in a 50 µm thick Teflon tape, darkened with one layer of black tape, and coupled to the SiPM with Xiameter PMX-200 silicone-based super-viscous (10^6 centistokes) optical grease, as shown in figure 3.

The detector packaging is valid in view of our tests (17.4 keV X-rays), but at lower energies (< 5 keV) the darkening tape stops a significant fraction of X-rays so another method should be implemented.

2.1 Readout

A Hamamatsu MPPC (SiPM) S13360-6050CS with a $50 \times 50\,\mu m^2$ pixel size is used for the measurements. At 25°C, when operated 3V over its breakdown voltage $V_{br} = 51.3$ V, its nominal gain is 1.7×10^6 and its photon detection efficiency (PDE) is 40%, at a peak sensitivity wavelength of 450 nm (close to the peak emission of EJ-200), while its breakdown voltage temperature coefficient is 54 mV/°C.

2023 JINST 18 T09007

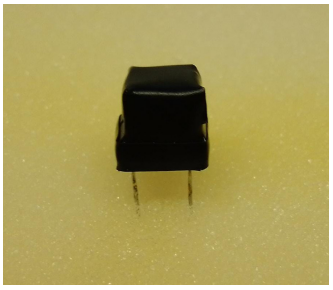

Figure 3. Picture of the detector, showing the scintillator (on top), coupled to the SiPM (below) with optical grease, wrapped with Teflon tape and darkened with black tape. Note that the SiPM pins distance is 7.4 mm.

2023 JINST 18 T09007

Pulses from the SiPM were amplified using a custom-built low-noise amplifier with a 600 gain and 80 MHz bandwidth. Data-taking is performed using a LeCroy Teledyne HDO6104 oscilloscope with sampling at 2.5 GS/s, and 1 GHz bandwidth. In order to suppress ambient pickup noise, in the offline analysis the waveforms are filtered, using the Python scipy library [7], with a digital IIR notch filter with a central frequency of 100 MHz and Q value of 1, followed by a Butterworth second-order low-pass filter with 200 MHz cutoff frequency [8].

For each waveform, the charge is evaluated as the integral from −20 to 420 ns with respect to the trigger, divided by the 50 Ω oscilloscope input impedance. As shown in figure 4, a dataset of 20000 dark count waveforms with a 20 mV trigger threshold was taken and analyzed to study the amplifier performances.

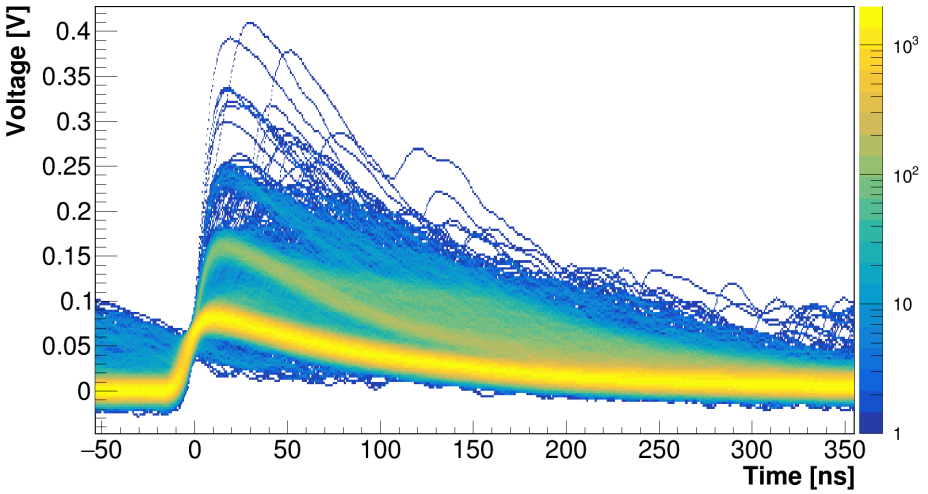

Figure 4. Dark count waveforms: the contributions from the single photoelectron populations can be appreciated (∼ 80 mV for each p.e.).

As shown in figure 5, from the charge spectrum of the dark count pulses, a mean charge of $Q_{PE} = 196.4 \pm 0.2$ pC can be estimated for the single photoelectron.

Then, knowing the amplifier gain (600), the gain of the SiPM can be estimated to be:

$$G_{\text{SiPM}} = \frac{Q_{PE}}{G_{\text{Amp}} e} = (2.04 \pm 0.01) \times 10^6 \tag{2.2}$$

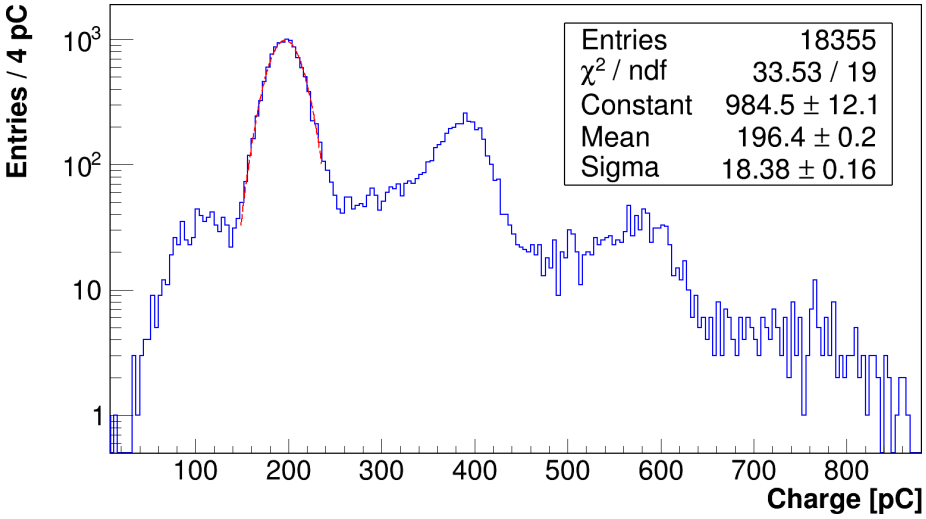

Figure 5. Charge spectrum of dark count pulses. The contributions from the different photoelectron peaks (up to 4) can be distinguished.

where $e = 1.602 \times 10^{-19} C$ is the elementary charge. Therefore the experimental value is compatible within 7% with the nominal SiPM gain of $G_{\text{SiPM}} = (1.91 \pm 0.01) \times 10^6$ at room temperature (18 ± 0.3°C).

3 Results

The detector was tested with a radioactive source, where α particles from a 10 mCi Am-241 source are directed to a molybdenum target in order to generate X-rays from Mo K-α and β lines. The X-ray flux is 2.4×10^4 photons/(s·sr) with an emission collimated to 0.5 sr and the relative intensity between K-β (19.63 keV) and K-α (17.44 keV) lines is 20%, therefore the average energy is 17.8 keV.

The analysis was based on a dataset of 20000 waveforms, taken with a trigger to 360 mV, corresponding to about 4.5 p.e. threshold, and with the X-ray source aperture touching the scintillator.

Thanks to the high gain of the amplifier, the different peaks corresponding to the photo-electrons are easily distinguishable, as shown in figure 6.

As expected, a linear relation between peak amplitude and the integrated charge is observed, as shown in figure 7.

The spectrum of the charge has been fitted, as shown in figure 8, with the sum, for each photoelectron peak $i = 1, 2, 3, \ldots$, of gaussian functions corresponding to the charge spectrum of the single photoelectrons peaks, weighted with the probability w_i of detecting i photoelectrons. The weights follow a gaussian in the i variable, with the mean (PE) corrisponding to the average number of photoelectrons and a σ_{PE} which includes all photostatistics fluctuations. The fit function is then:

$$f(Q) \propto \sum_i \text{Gaus}\,(i, PE, \sigma_{PE}) \cdot \text{Gaus}\left(Q, Q_{PE} \cdot i, \sqrt{Q_{\text{Noise}}^2 + i \cdot (Q_{PE} \cdot GF)^2}\right) \tag{3.1}$$

where Q_{PE} is the mean charge for one photoelectron, Q_{Noise} is the equivalent charge noise and GF is the single-cell (one photoelectron) relative gain spread of the SiPM.

2023 JINST 18 T09007

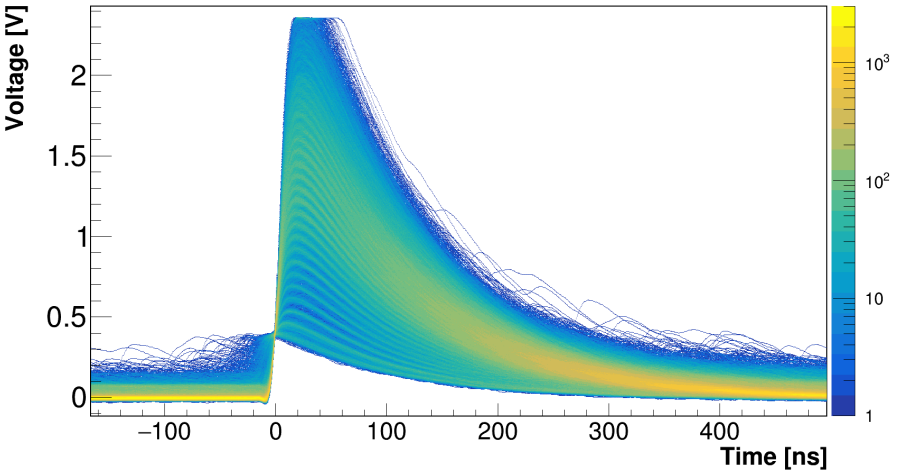

Figure 6. Histogram of waveforms for data taken with the molybdenum K lines.

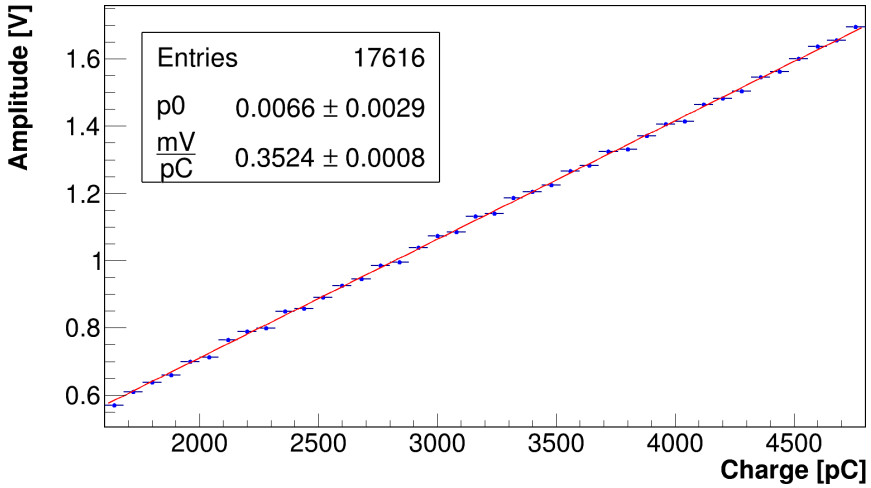

Figure 7. Charge vs. amplitude profile histogram, with linear regression.

A mean value of about 20 photoelectrons per X-ray photon is obtained, i.e. a photoelectron yield of 1.13 photoelectrons/keV, which when divided by the SiPM PDE (∼ 40%), corresponds to 2.9 optical photons/keV reaching the SiPM.

Moreover, from the fit, an energy resolution of $\sigma_{PE}/PE = 28\%$ is obtained, to be compared with the photostatistics spread $1/\sqrt{PE} = 22\%$. Then, the additional fluctuation of 17% must be included in order to get the correct resolution — this spread might be due to the geometrical spread of photons inside the scintillator and to the fact that the X-rays are impinging in different points of the scintillator with different directions. As verified with a simple Monte Carlo simulation, the presence of two different lines with a relative intensity of 20% and a difference in energy of 2.2 keV does not significantly affect the resolution.

In any case, the data show a large charge/photoelectrons conversion factor of $Q_{PE} \sim 196$ pC, a very good (∼ 40 pC) equivalent charge noise after amplification of factor 600, and a low intrinsic SiPM single-cell gain spread of GF ∼ 6%.

2023 JINST 18 T09007

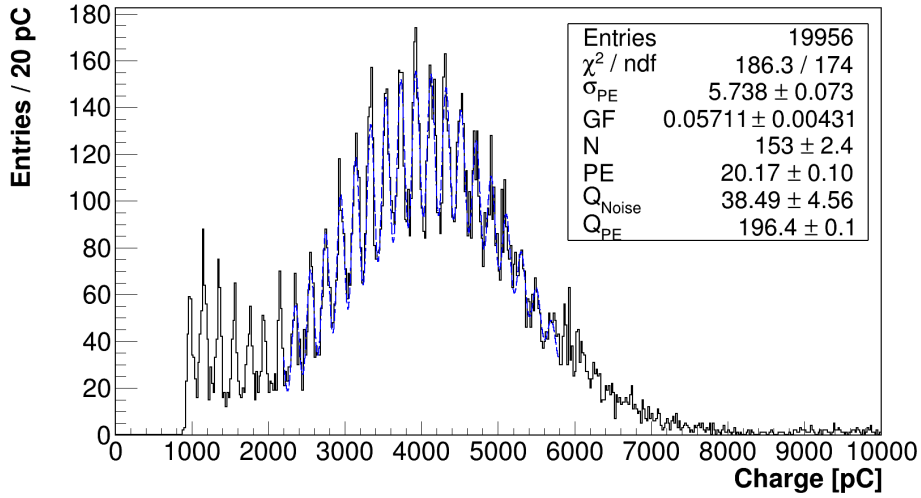

Figure 8. Charge spectrum for data taken with the molybdenum K lines with a 360 mV trigger threshold, fitted with $f(Q)$.

3.1 Simulation

In order to roughly estimate the light yield in the energy range used in this work, the detector was simulated with Geant4 [9] using the low-energy electromagnetic Livermore physics list, shooting 17.44 keV X-rays (molybdenum K-α line) towards the scintillator, which has the same size as the real one. For each event, the total absorbed energy (above a 3 keV threshold) and the energy of the hardest scattered electron was saved, as shown in figure 9.

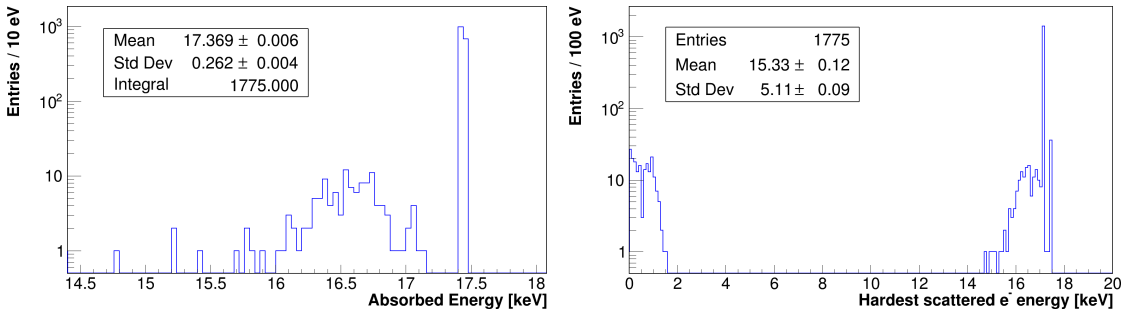

Figure 9. Geant4 simulation results: absorbed energy spectrum from 17.44 keV X-rays with a 3 keV threshold (left) and energy spectrum of hardest scattered electrons, with a peak at 17.15 keV (right).

In most cases, the photons interact with a carbon atom through photoelectric effect, scattering a $\sim$ 17.15 keV energy electron. As expected, the energy difference is close to the carbon 1s absorption peak (285 eV). In other cases, as shown in figure 9, the photons interact through incoherent or coherent scattering, so they only deposit a small fraction of their initial energy. In EJ-200, the 17.15 keV scattered electrons have a stopping power of $dE/dx = 14.63\,\mathrm{MeV\,cm^2/g}$ (around 7 times its value for MIPs), so the light yield quenching must be taken into account, as dictated by Birks' Law:

$$\frac{dL}{dx} = S\frac{\frac{dE}{dx}}{1 + kB\frac{dE}{dx}} \tag{3.2}$$

2023 JINST 18 T09007

where $\frac{dL}{dx}$ is the differential number of photons per length, $S = 10^4$ photons/MeV is the nominal light yield of EJ-200 and $kB = 2 \times 10^{-2}\,\mathrm{g\,MeV^{-1}\,cm^{-2}}$ is the Birks' coefficient for polyvinyl-toluene-based scintillators [10].

The Birks' law formula can be integrated in dx, as follows:

$$L = S \int_0^R \frac{\frac{dE}{dx}}{1 + kB\frac{dE}{dx}} dx \tag{3.3}$$

where R is the scattered electron range in EJ-200, and $E_0 = 17.15\,\mathrm{keV}$ is its initial energy. The integral is numerically evaluated, event-by-event, directly in the Geant4 simulation, to get the histogram of the number of optical photons generated in the scintillator (without including any smearing due to Poisson photostatistics), as shown in figure 10.

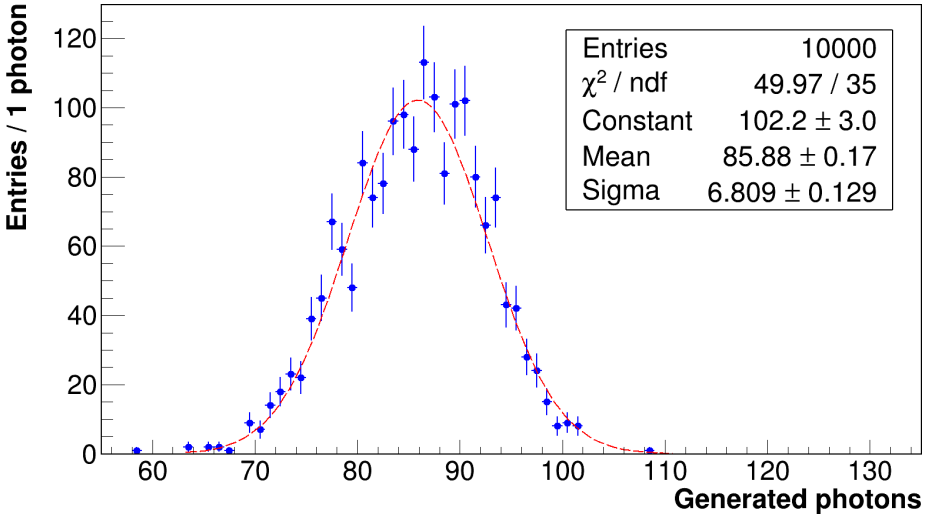

Figure 10. Simulated histogram of the number of optical photons generated in the scintillator, with a threshold at 50 photons. The spread is due to fluctuations in energy loss.

According to the simulation, the mean number of optical photons generated is 85.71 ± 0.16, which translates into a mean light yield of 4.9 photons/keV. By comparing this value with the number of optical photons reaching the SiPM estimated before (2.9/keV), a reasonable ∼ 60% light collection efficiency is estimated.

4 Conclusion

An X-ray detector for low energies was built and operated, featuring a plastic scintillator coupled to a SiPM and showed optical photon-counting capabilities. The detector was tested using X-rays coming from molybdenum K lines and showed overall good performance. An energy resolution of 28%, with 1.13 photoelectrons per keV, is obtained. An additional fluctuation of 17% is present along with the photostatistics, and it will be further investigated using different X-ray energies.

Future tests will also be performed using a 2 mm thick GAGG(Ce) crystal [11], featuring a 60 photons/keV light yield, a 6.63 g/cm^3 density and a 0.6 mm X-ray absorption length at 30 keV. The use of GAGG should allow a more efficient detection of X-rays and a better resolution.

2023 JINST 18 T09007

References

[1] EJ-200 datasheet, https://eljentechnology.com/images/products/data_sheets/EJ-200_EJ-204_EJ-208_EJ-212.pdf.

[2] J.H. Hubbell, *Photon Cross Sections, Attenuation Coefficients and Energy Absorption Coefficients from 10 keV to 100 GeV*, Natl. Stand. Ref. Data Ser., Nat. Bur. Stand. (U.S.) 29 (1969).

[3] S. M. Tajudin, Y. Namito, T. Sanami and H. Hirayama, *Response of plastic scintillator to gamma sources*, *Appl. Radiat. Isot.* **159** (2020) 109086.

[4] Hamamatsu MPPC S13360 series datasheet, https://www.hamamatsu.com/content/dam/hamamatsu-photonics/sites/documents/99_SALES_LIBRARY/ssd/s13360_series_kapd1052e.pdf.

[5] M.J. Berger, J.S. Coursey, M.A. Zucker and J. Chang, *ESTAR, PSTAR, and ASTAR: Computer programs for calculating stopping-power and range tables for electrons, protons, and helium ions*, National Institute of Standards and Technology, Gaithersburg, U.S.A. (1992), http://physics.nist.gov/Star.

[6] C.T. Chantler, *Detailed tabulation of atomic form factors, photoelectric absorption and scattering cross section, and mass attenuation coefficients in the vicinity of absorption edges in the soft X-ray* ($Z = 30-36,\ Z = 60-89,\ E = 0.1-10\,keV$) *— addressing convergence issues of earlier work*, *J. Synchrotron Radiat.* **8** (2001) 1124.

[7] P. Virtanen et al., *SciPy 1.0 — Fundamental Algorithms for Scientific Computing in Python*, *Nature Meth.* **17** (2020) 261 [arXiv:1907.10121].

[8] S.J. Orfanidis, *Introduction To Signal Processing*, Prentice-Hall (1996).

[9] GEANT4 collaboration, *GEANT4 — a simulation toolkit*, *Nucl. Instrum. Meth. A* **506** (2003) 250.

[10] L. Torrisi, *Plastic scintillator investigations for relative dosimetry in proton-therapy*, *Nucl. Instrum. Meth. B* **170** (2000) 523.

[11] Y. Zhu et al., *Scintillation properties of GAGG:Ce ceramic and single crystal*, *Opt. Mater.* **105** (2020) 109964.

2023 JINST 18 T09007